Dimensional Synthesis of Parallel Robots: Unified Kinematics and Dynamics using Full Kinematic Constraints

Maßsynthese für Parallele Roboter: Einheitliche Kinematik und Dynamik mit vollständigen kinematischen Zwangsbedingungen

Moritz Schappler, Prof. Dr.-Ing. Tobias Ortmaier, Leibniz Universität Hannover, Institut für Mechatronische Systeme, Appelstraße 11a, 30167 Hannover, Deutschland. Korrespondenz: moritz.schappler@imes.uni-hannover.de.

Abstract

A variety of different structures for parallel kinematic machines (PKM) have been found by means of systematic structural synthesis. To find the structure that is suited best for a specific task, an efficient and generic selection method is necessary. For simple structures with multi-degree-of-freedom joints like the Gough-Stewart robot, methods for modeling and dimensional optimization are well established. Less methods are available for more complex structures with single-degree-of-freedom joints. This contribution combines general approaches for the modeling of the kinematics and dynamics of parallel robots to obtain an efficient dimensional synthesis of PKM.

Kurzfassung

Durch systematische Struktursynthese wurden bislang eine Vielzahl unterschiedlicher parallelkinematischer Maschinen (PKM) beschrieben. Um die passendste Roboterkinematik für eine gegebene Aufgabe zu finden, ist eine effiziente und allgemeingültige Auswahlsystematik erforderlich. Für einfache Systeme mit mehrwertigen Gelenken wie die Gough-Stewart-PKM liegen bereits Modellierungs- und Optimierungsverfahren vor. Für komplexere Strukturen mit mehr einwertigen Gelenken ist die Auswahl an Verfahren eingeschränkter. Der vorliegende Beitrag führt allgemeine Ansätze für die Modellierung der Kinematik und Dynamik zusammen, um die Maßsynthese von PKM besonders effizient zu gestalten.

1 Introduction

The structural synthesis of parallel robots by means of screw theory [1] or evolutionary morphology [2] has produced a variety of different architectures. However, for only few of them a specific application has been found despite numerous research demonstrators focusing on single aspects of the robots [3]. It is well established that the theoretical advantages of parallel robots are strongly dependent on their dimensioning [3]. An automatic dimensioning (i.e. dimensional synthesis) for all existing types of robots is necessary to select the robot that is suited best for a specific given application. Therefore, the aspect of selecting a structure (structural synthesis) and choosing specific parameter values (dimensional synthesis) should be performed in a combined structural and dimensional synthesis [4]. Efforts on the dimensional synthesis constitute a major part in the research of parallel robots, beginning in the early 2000s driven by international robotics research groups, e.g. [3, 5], and German researchers in the field of machine tools, e.g. [4, 6–8]. Until today, research is focused mainly on parallel robots with leg chains with the minimal amount of links and joints with multiple degrees of freedom (DoF), like universal and spherical joints. This has advantages regarding the stiffness, which is essential for machining tasks [7].

Only few authors report a dimensional synthesis for multiple different robots with the ambition to compare them by this means, e.g. [4] in a case study for two different architectures of Delta robots or [10] for serial robots. Most authors perform the dimensional synthesis for specific structures, such as the Delta robot [11, 12], the Hexa robot [4, 6], the CaPaMan [5] or a cable-driven ankle rehabilitation robot in [13]. The synthesis is mainly focused on kinematic characteristics such as workspace and conditioning of the Jacobian or kinetostatic characteristics such as the stiffness [5, 12]. The dynamics of the parallel robot is only regarded in some cases, e.g. by taking the minimal possible acceleration of the machine as a constraint [4]. A partly consideration of dynamics aspects is performed by assessing the condition number of the mass matrix in [12] or the Eigen frequencies of the robot obtained from the mass and stiffness matrix in [13]. In the dimensional synthesis of serial robots more attention is paid to the dynamics, e.g. by [14] using a multi-body simulation tool like ADAMS in the optimization loop. A consideration of material stress and internal forces is to the best knowledge of the authors only performed in the dimensional synthesis of serial robots, e.g. by [15] who perform FE analyses with ANSYS for a parametric CAD model inside the optimization loop.

Usually, a heuristic multi-objective optimization is performed in the dimensional synthesis, e.g. with the Strength Pareto Evolutionary Algorithm [4, 12] or the Nondominated Sorting Genetic Algorithm [13]. Using a weighted sum to incorporate multiple objectives is prone to the subjectivity of the user [3, 13].

To be able to perform a dynamics-based optimization of general parallel robots without assumptions on the joint

types, this paper addresses a general and efficient formulation of the optimization problem. The contributions of the paper are

- the application of a general kinematic and dynamics model on the dimensional synthesis of non-conventional parallel robots,
- the proposition of an efficient optimization structure,
- simulative results and their discussion.

The remainder of the paper is structured as follows: The general model of the kinematics and dynamics is presented in Sec. 2. The structure for defining the optimization problem of the dimensional synthesis is sketched in Sec. 3 followed by the results in Sec. 4 and a summary in Sec. 5.

2 System Description and Model

The general parallel robot model subject to the dimensional synthesis in this paper consists of m leg chains with n_i joints each, which support the moving platform with respect to a fixed base. A sketch of the robot is depicted in Fig. 2 with the necessary coordinate systems ("CS") for kinematic modeling, including a base frame $(\mathrm{CS})_0$ of the PKM and base frames $(\mathrm{CS})_{A_i}$ and virtual end effectors $(\mathrm{CS})_{E_i}$ for the leg chains. The definition of the coupling frames $(\mathrm{CS})_{B_i}$ on the platform allow arbitrary alignments of legs and platform. The moving platform frame $(\mathrm{CS})_P$ is expressed with the minimal coordinates $\mathbf{x}$ containing the Cartesian position $\mathbf{x}_\mathrm{t}$ and orientation $\mathbf{x}_\mathrm{r}$ (as three Euler angles). The joint coordinates $\mathbf{q}_i$ of each leg chain i are stacked as

$$\mathbf{q}^\mathrm{T} = (\mathbf{q}_1^\mathrm{T}, \cdots, \mathbf{q}_m^\mathrm{T}) \quad \text{with} \quad \mathbf{q}_i^\mathrm{T} = (q_{i,1}, \cdots, q_{i,n_i}). \tag{1}$$

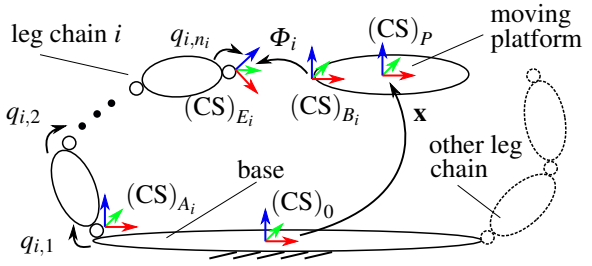

Figure 2 Sketch of the general parallel robot kinematics

This general model extends the textbook formulations [3, 16] by including passive *and* coupling joints to avoid assumptions on the solvability of the kinematic equations ("minimal kinematics set", [3]). The following sections introduce the unified kinematic (Sec. 2.1) and dynamics (Sec. 2.2) modeling, which leads to the internal forces (Sec. 2.4) and energy (Sec. 2.5) used in the dimensional synthesis of parallel robots, as sketched in Fig. 1.

2.1 Full Kinematic Constraints

To be able to solve the inverse kinematics problem for all active and passive joint coordinates $\mathbf{q}$, a full set of kinematic constraints has to be defined to generate a determined system of equations. In the context of dimensional synthesis, a trajectory of the platform pose $\mathbf{x}(t)$ is given and has to be accomplished by the simulated parallel robot. These constraints can e.g. be defined as vector loops between the respective leg chains [2] or one leg and the platform [3]. The formulation of the full kinematic constraints on position level instead of velocity level has the advantage of providing a feasible residual for a gradient-based solution of the inverse kinematics problem [9]. The translational part of the full kinematic constraints can be formulated as the difference of the coupling point position B_i on the platform and the corresponding coupling joint E_i on the leg chain i with

$$\boldsymbol{\Phi}_{\mathrm{t},i}(\mathbf{q}_i, \mathbf{x}) = -\mathbf{r}_{A_iB_i}(\mathbf{x}) + \mathbf{r}_{A_iB_i}(\mathbf{q}_i) \stackrel{!}{=} \mathbf{0}, \tag{2}$$

as established in the state of the art [3] and sketched in Fig. 2. The minimal form of the rotational part of the kinematic constraints is calculated with the Euler angles ϕ_{XYZ} of the rotational difference of the frames $(\mathrm{CS})_{E_i}$ on the leg chain i and the corresponding $(\mathrm{CS})_{B_i}$ on the platform, with

$$\boldsymbol{\Phi}_{\mathrm{r},i}(\mathbf{q}_i, \mathbf{x}) = \phi_{XYZ}\left({}^0\mathbf{R}_{B_i}^\mathrm{T}(\mathbf{x}_\mathrm{r}) {}^0\mathbf{R}_{E_i}(\mathbf{q}_i)\right) \stackrel{!}{=} \mathbf{0}, \tag{3}$$

as elaborated in detail in [9]. The kinematic constraints for the whole robot are then stacked with the terms for the single leg chains to

$$\boldsymbol{\Phi}^\mathrm{T} = (\boldsymbol{\Phi}_1^\mathrm{T}, \cdots, \boldsymbol{\Phi}_m^\mathrm{T}), \quad \text{with} \quad \boldsymbol{\Phi}_i^\mathrm{T} = (\boldsymbol{\Phi}_{\mathrm{t},i}^\mathrm{T}, \boldsymbol{\Phi}_{\mathrm{r},i}^\mathrm{T}). \tag{4}$$

The full inverse Jacobian of the parallel robot

$$\tilde{\mathbf{J}}^{-1} = -\left(\frac{\partial \boldsymbol{\Phi}}{\partial \mathbf{q}}\right)^{-1} \left(\frac{\partial \boldsymbol{\Phi}}{\partial \mathbf{x}}\right) \quad \text{with} \quad \dot{\mathbf{q}} = \tilde{\mathbf{J}}^{-1}\dot{\mathbf{x}} \tag{5}$$

is obtained by time differentiation of the constraint equation (4) and relates the velocities $\dot{\mathbf{q}}$ of all joints and the platform $\dot{\mathbf{x}}$. To extract only the velocity $\dot{\mathbf{q}}_\mathrm{a}$ of the actuated joints, the corresponding rows in $\dot{\mathbf{q}}$ are extracted with the selection matrix $\mathbf{P}_\mathrm{a}$ with

$$\mathbf{q}_\mathrm{a} = \mathbf{P}_\mathrm{a}\mathbf{q} \quad \text{and} \quad \mathbf{J}^{-1} = \mathbf{P}_\mathrm{a}\tilde{\mathbf{J}}^{-1}, \tag{6}$$

giving the analytic Jacobian of the parallel robot, which is square for non-redundant robots. The joint accelerations can be obtained by differential calculus as

$$\ddot{\mathbf{q}} = \tilde{\mathbf{J}}^{-1}\ddot{\mathbf{x}} + \dot{\tilde{\mathbf{J}}}^{-1}\dot{\mathbf{x}}. \tag{7}$$

The partial derivatives in (5) can be partly calculated in analytic form, as described in [9].

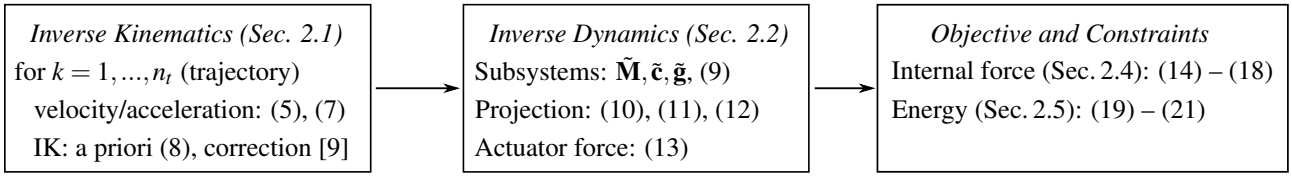

Figure 1 Unified calculation of the inverse kinematics and inverse dynamics for application in the dimensional synthesis

The inversion of the 36×36-matrix $\partial \Phi / \partial \mathbf{q}$ (in the full-mobility case) should be performed numerically. The derivatives of the terms required for (7) can also be partly calculated symbolically.
For an efficient calculation of the whole robot trajectory for time step k with $t = k\Delta t$ with $k = 1, ..., n_t$, the relation

$$\mathbf{q}_{k+1} = \mathbf{q}_k + \dot{\mathbf{q}}_k \Delta t + \frac{1}{2} \ddot{\mathbf{q}}_k \Delta t^2 \tag{8}$$

can be used as an initial value for the gradient-based solution of the inverse kinematics problem [17], [9].

2.2 Unified Kinematics and Dynamics

To be able to determine the energy consumption of an arbitrary parallel robot for a given reference trajectory in the dimensional synthesis, the inverse dynamics is required. The application of the principle of energy equivalence for parallel robots from [18, 19] has to be extended using the full kinematic constraints from the previous section. The formulation from Abdellatif et al. [18] only applies for parallel robots which can be described solely with translational constraints (2), i.e. robots with leg chains containing at most two links and ending in spherical joints in the full mobility case. Some of the the robots resulting from the structural synthesis from Gosselin et al. [1] and Gogu et al. [2] do not meet this requirement.
Following the more general approach from Do Thanh et al. [19] the parallel robot is decomposed into the subsystems leg chains and platform. The inverse dynamics for the subsystems in their respective minimal coordinates $\mathbf{q}_i$ and $\mathbf{x}$ can be obtained with standard methods such as the Lagrange equations. The resulting terms of the explicit dynamics equation can be assembled as the block-diagonal full inertia matrix $\tilde{\mathbf{M}}$ and stacked as the full Coriolis and centrifugal forces vector $\tilde{\mathbf{c}}$ and gravitational forces vector $\tilde{\mathbf{g}}$. The implicit form $\tilde{\tau}$ of the dynamics can be assembled as the sum of the single terms as

$$\tilde{\tau} = \tilde{\mathbf{M}}[\ddot{\mathbf{q}}^{\mathrm{T}}, \ddot{\mathbf{x}}^{\mathrm{T}}]^{\mathrm{T}} + \tilde{\mathbf{c}} + \tilde{\mathbf{g}}. \tag{9}$$

By applying the principle of D'Alembert, the dynamics of the subsystems can be projected into the minimal coordinates $\mathbf{x}$ of the parallel robot. To this end, the Jacobian matrix from the inverse kinematics step in (5) is extended by a unit matrix corresponding to the platform coordinates to obtain the projection matrix

$$\tilde{\mathbf{D}}^{\mathrm{T}} = \left(\tilde{\mathbf{J}}^{-\mathrm{T}}, \mathbf{1} \right). \tag{10}$$

The projection of the dynamics gives

$$\mathbf{M} = \tilde{\mathbf{D}}^{\mathrm{T}} \tilde{\mathbf{M}} \tilde{\mathbf{D}}, \quad \mathbf{c} = \tilde{\mathbf{D}}^{\mathrm{T}} (\tilde{\mathbf{M}} \dot{\tilde{\mathbf{D}}} \dot{\mathbf{x}} + \tilde{\mathbf{c}}), \tag{11}$$

$$\mathbf{g} = \tilde{\mathbf{D}}^{\mathrm{T}} \tilde{\mathbf{g}} \quad \text{and} \quad \tau = \tilde{\mathbf{D}}^{\mathrm{T}} \tilde{\tau}. \tag{12}$$

To reduce the computational effort, the implicit form τ of the inverse dynamics in (12) should be used. This avoids the explicit computation of the inertia and Coriolis terms in (11), which are not used in the dimensional synthesis, unless investigations on inertial forces [8] or Eigen frequencies [13] require the inertia matrix $\mathbf{M}$. Furthermore, this allows neglecting the matrix $\dot{\tilde{\mathbf{J}}}^{-1}$ in (7), which has low influence on the kinematics. The actuator forces for the calculation of the power consumption of the parallel robot are obtained with the inverse Jacobian from (6) as

$$\tau_{\mathrm{a}} = \mathbf{J}^{-\mathrm{T}} \tau = \mathbf{J}^{-\mathrm{T}} (\mathbf{M} \ddot{\mathbf{x}} + \mathbf{c} + \mathbf{g}). \tag{13}$$

2.3 Discussion on Velocity Constraints

Using D'Alembert's principle ("virtual work"), as proposed in [19] requires the definition of kinematic constraints at the position level, which demands some additional efforts for the orientation [9]. By defining the constraints on velocity level [2], the calculation of the Jacobian is simplified by being able to use angular velocities and corresponding geometric Jacobians instead of Euler angles and their gradient matrices [20]. The dynamics are then effectively obtained with Jourdain's principle ("virtual power"), leading to the same result [20].

2.4 Internal Forces in Parallel Robots Legs

For an evaluation of the mechanical stress in the structure of the parallel robots legs, the internal forces and moments have to be known. The projection-based dynamics does not produce cutting forces, since they do not perform work, except in actuated joints. Using the Newton-Euler algorithm would provide these forces, but requires setting up a large system of equations and is therefore only applicable to specific mechanisms such as the Gough-Stewart robot [3]. Therefore, the internal forces are reconstructed by adapting the procedure presented in [21].
With the known joint velocity $\dot{\mathbf{q}}_i$ and acceleration $\ddot{\mathbf{q}}_i$ from (5) and (7) for all active and passive joints of the leg chain i, the stacked forces and moments

$$\mathbf{w}_{i,\mathrm{int}}(\mathbf{q}_i, \dot{\mathbf{q}}_i, \ddot{\mathbf{q}}_i) = (\mathbf{w}_{i,1,\mathrm{int}}^{\mathrm{T}}, \cdots, \mathbf{w}_{i,n_i,\mathrm{int}}^{\mathrm{T}})^{\mathrm{T}} \tag{14}$$

from the internal dynamics can be computed with the recursive Newton-Euler algorithm [17, 20]. As sketched in Fig. 3, the single leg chain i cut open at the platform can be regarded as a serial link chain with an external wrench $\mathbf{w}_{B_i}$ acting at the last link, giving the dynamics equation

$$\tau_i = \mathbf{M}_i \ddot{\mathbf{q}}_i + \mathbf{c}_i + \mathbf{g}_i = \tau_{\mathrm{m},i} + \mathbf{J}_i^{\mathrm{T}} \mathbf{w}_{B_i}, \tag{15}$$

where τ_i is equal to the elements of $\mathbf{w}_{i,\mathrm{int}}$ corresponding to the respective actuated joint [17].

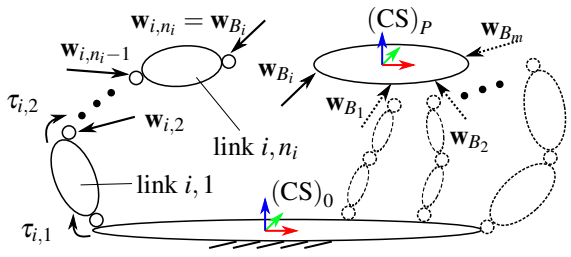

Figure 3 Internal forces in the leg chains of the parallel robot.

The Jacobian $\mathbf{J}_i$ projects the external wrench $\mathbf{w}_{B_i}$ (from perspective of the cut open leg chain) into the joint space coordinates $\mathbf{q}_i$ of the leg chain. By assuming neither redundancy nor singularity, (15) can be rewritten to

$$\mathbf{w}_{B_i} = (\mathbf{f}_{B_i}^{\mathrm{T}}, \mathbf{m}_{B_i}^{\mathrm{T}})^{\mathrm{T}} = \mathbf{J}_i^{-\mathrm{T}} (\tau_i - \tau_{\mathrm{m},i}), \tag{16}$$

yielding the cut force $\mathbf{f}_{B_i}$ and moment $\mathbf{m}_{B_i}$ in the coupling point B_i. The vector of motor torques $\tau_{\mathrm{m},i}$ in the leg chain has zeros for passive joints and the corresponding entry $\tau_{\mathrm{a},i}$ from (13). The cut wrenches in all joints of the leg chain i induced by the parallel coupling are obtained by

$$\mathbf{w}_{i,\mathrm{coupl}} = \mathbf{J}_{i,\mathrm{full}}^{\mathrm{T}} \mathbf{w}_{B_i}, \tag{17}$$

using the full geometric Jacobian $\mathbf{J}_{i,\mathrm{full}}$ of the leg chain. Equivalent to (15), the cut wrench in the joints (with the effect of internal dynamics *and* coupling forces) results to

$$\mathbf{w}_i = \mathbf{w}_{i,\mathrm{int}} - \mathbf{w}_{i,\mathrm{coupl}} = (\mathbf{w}_{i,1}^{\mathrm{T}}, \cdots, \mathbf{w}_{i,n_i}^{\mathrm{T}})^{\mathrm{T}}. \tag{18}$$

2.5 Energy Consumption

It is assumed that all electric drives of the actuated joints can exchange power in a common DC link, which is the case for newly installed robots, and enables improving energy efficiency in industrial production. The mechanical power of the single robot actuators can be summed up (assuming no losses) to the electric DC link power

$$P_{\mathrm{link}} = \tau_{\mathrm{a}}^{\mathrm{T}} \dot{\mathbf{q}}_{\mathrm{a}}. \tag{19}$$

Assuming no energy storage or recuperation, the electric power required from the grid results to

$$P_{\mathrm{grid}} = \begin{cases} P_{\mathrm{link}}, & P_{\mathrm{link}} > 0 \\ 0, & \text{otherwise.} \end{cases} \tag{20}$$

By integrating the power over time with

$$E_{\mathrm{grid}} = \int_0^{T_{\mathrm{Traj}}} P_{\mathrm{grid}} \, \mathrm{d}t \tag{21}$$

the energy consumption of the parallel robot in the reference trajectory can be obtained.

3 Optimization

The dimensional synthesis of parallel robots is implemented as a global optimization of the kinematic parameters of the robot. As reasoned in [10, 13], performing a multi-objective optimization requires selecting a solution on the Pareto hyper-surface of all different objective criteria. When trying to select the best robot architecture from many possibilities for a given task, an unambiguous criterion has to be used, not requiring a human decision [10] or trial-and-error on weighting factors of different criteria [13]. Therefore, a single-objective optimization is performed, where the energy consumption is used as an exemplary criterion and different constraints are used. The particle swarm optimization is employed since it has, together with the genetic algorithm, proven to be efficient for this kind of design problem. In the following, the problem formulation is elaborated in Sec. 3.1, the definition of the robot parameters is described in Sec. 3.2 and the objective function and the various constraints are defined in Sec. 3.3 and Sec. 3.4.

3.1 Formulation of the Problem

The ambition of the design optimization is to find the set of robot parameters ("particle") $\mathbf{p}_{\mathrm{opt}}$, which minimizes the fitness function $f(\mathbf{p})$, leading to an optimal design. Many parameter combinations however do not present a valid solution, since they violate some constraint. The bottleneck in the optimization process is the computation time. Therefore, an efficient way of handling the constraints is to abort the processing of a particle once one of the constraints is not met. From the different possibilities of including constraints in the optimization [22], an adaption of the static penalty approach is used which is termed "hierarchical constraints" in this paper. Following [10], the penalty terms v_i are defined hierarchically according to the infeasibility of the solution with

$$v_1(\mathbf{p}) > v_2(\mathbf{p}) > \cdots > z(\mathbf{p}), \tag{22}$$

where z represents the objective function and v_i the penalty terms for the constraints, which are included in the piecewise definition of the fitness function f, depicted in Fig. 4. To increase the convergence of the optimization as opposed to constant penalties e.g. used in [10], the degree of violation $\rho > 0$ of the constraints is included in the penalties v_i and normalized with the function

$$f_{\mathrm{norm}}(\rho) = \frac{2}{\pi} \arctan(\rho / \rho_{\mathrm{scale}}) \tag{23}$$

to the range of 0 to 1. Since it is not always possible to determine the upper limit of ρ for any kind of parameter values, the saturation of (23) ensures that each constraint penalty v_i has a dedicated range in the possible values for the fitness function f. The scaling ρ_{scale} adjusts the range of the values of ρ which lie in the saturation of $f_{\mathrm{norm}} \approx 1$.

3.2 Definition of Parameters

To reduce the nonlinearity of the fitness f function with respect to the optimization parameters $\mathbf{p}$, a conversion between optimization parameters and physical kinematic parameters of the robot is performed. The measure especially aims at reducing the coupling between parameters. Therefore, the following meta-parameters of the optimization are introduced:

- the scaling parameter p_{scale} increases the size of the whole robot (platform and legs) without changing its overall kinematics characteristics,
- the platform scaling parameter p_{plfscale} scales the diameter of the moving platform relative to the base.

The kinematic parameters $\mathbf{p}_{\mathrm{kin}}$ of the parallel robots are

- the base diameter $d_{\mathrm{base}} = p_{\mathrm{scale}} p_{\mathrm{base}}$,
- the platform diameter $d_{\mathrm{plf}} = p_{\mathrm{plfscale}} d_{\mathrm{base}}$,
- the distance $d_{\mathrm{basepairdist}} = d_{\mathrm{base}} p_{\mathrm{bpdscale}}$ of coupling point pairs with scaling p_{bpdscale}, in case of a pairwise alignment at the base (Fig. 5,a),
- the pair distance $d_{\mathrm{plfpairdist}} = d_{\mathrm{plf}} p_{\mathrm{ppdscale}}$ with scaling p_{ppdscale} for the moving platform (Fig. 5,a,b),
- the elevation α_{Pyr} of the base coupling joint, in case of a pyramidal alignment of the first joint axis of the leg chains (Fig. 5,a,b),
- the Denavit-Hartenberg-parameters for links $1 \leq i \leq n_i$, $\alpha_{i,\mathrm{DH}} = p_{\alpha_i}$, $a_{i,\mathrm{DH}} = p_{\mathrm{scale}} p_{a_i}$, $\theta_{i,\mathrm{DH}} = p_{\theta_i}$ and $d_{i,\mathrm{DH}} = p_{\mathrm{scale}} p_{d_i}$, describing the serial link leg chains kinematics.

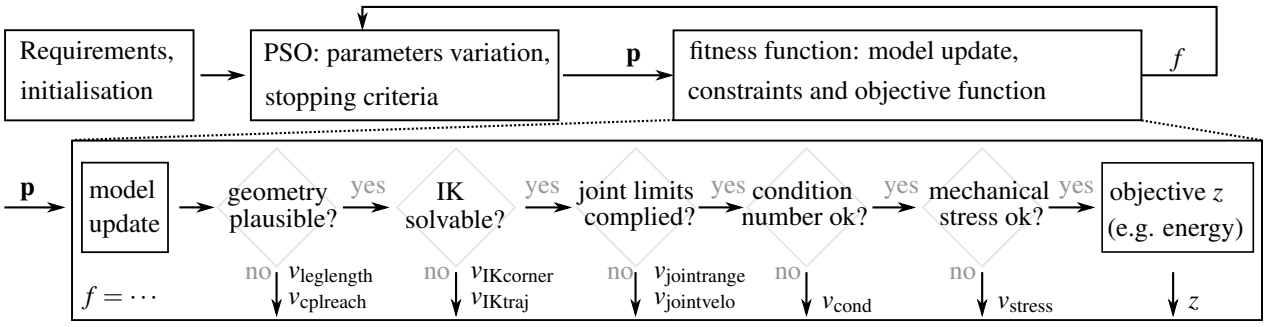

Figure 4 Overview of the PSO optimization and the structure of the fitness function with hierarchichal constraints.

Depending on the base and platform morphology (circular, pair-wise, pyramidal) and the kinematics of the symmetric legs, a different number of kinematic parameters

$$\mathbf{p}_{\text{kin}} = [d_{\text{base}}, d_{\text{plf}}, d_{\text{basepairdist}}, \cdots, d_{n_i,\text{DH}}]^{\text{T}} \tag{24}$$

and corresponding optimization parameters

$$\mathbf{p} = [p_{\text{scale}}, p_{\text{base}}, p_{\text{plfscale}}, p_{\text{bpdscale}}, \cdots, p_{d_{n_i}}]^{\text{T}} \tag{25}$$

are subject to the optimization.

3.3 Objective Function

Since the energy consumption of the parallel robot for a reference trajectory is a scalar value and is correlated with other criteria such as moved mass and joint speeds, it is well suited for an objective function of the dimensional synthesis. The range of values for the energy from (21) is not known in advance. The objective function

$$z = f_{\text{norm}}(E_{\text{grid}}) \tag{26}$$

is therefore constructed by normalizing and saturating the energy value with the function from (23).

3.4 Constraints

As introduced in Sec. 3.1, a hierarchy of constraints is assumed [10] which extends the classical problem formulation in constrained optimization, where all constraints are handled equally as equality or inequality constraints [22].

3.4.1 Geometric Feasibility

First, the geometric feasibility of the parallel robot kinematic parameters is tested. If the legs are too short to close the distance between base and platform radius, the first constraint penalty $v_{\text{leglength}}$ is set. If the coupling point B_i is not reachable with the maximum length of a leg chain for any corner point of the workspace, the second penalty v_{cplreach} is set to a value corresponding to the longest missing leg length.

3.4.2 Inverse Kinematics of Points and Trajectory

Next, the inverse kinematics is solved for all corner points of the workspace. The mean remaining violation of the kinematic constraints Φ serves as a penalty v_{IKcorner}. If this remains below the tolerance, i.e. all corner points are reachable in the desired orientation, the inverse kinematics for the reference trajectory of the optimization is calculated. The first erroneous trajectory sample k_{err} in relation to the trajectory length n_t serves as a penalty value v_{IKtraj}.

3.4.3 Joint Limits: Range, Velocity, Configuration

For the obtained joint trajectory $\mathbf{q}(t)$ constraints on the feasibility regarding joint motion are checked. First, limits on the joint range

$$\mathbf{q}_{\text{range}} = \max_t \mathbf{q}(t) - \min_t \mathbf{q}(t) \tag{27}$$

are tested, where for revolute joints the 2π-periodicity is regarded with an extended algorithm for (27). The allowed range of motion $\mathbf{q}_{\text{range,max}}$ of revolute joints can be set lower for universal and spherical joints than for single-DoF revolute joints. The maximum exceedance relative to the respective range results in the penalty term $v_{\text{jointrange}}$. Exceeding the maximum joint velocity $\dot{\mathbf{q}}_{\text{max}}$ results in the penalty $v_{\text{jointvelo}}$ and already indicates a bad-conditioned Jacobian. Since a flipping of joint configurations ("elbow up/down") can not be completely prevented in the gradient-based inverse kinematics, the difference between the numeric differentiation of the joint positions $\mathbf{q}(t)$ from the inverse kinematics and the velocities from the Jacobian in (5) are taken as a penalty $v_{\text{configflip}}$.

3.4.4 Condition Number of the Jacobian

If the joint trajectory has proven valid in the previous steps, the condition number of the Jacobian from (6) is calculated for all samples of the trajectory. If the condition number for any sample exceeds a threshold, this leads to the penalty

$$v_{\text{cond}} = f_{\text{norm}}(\log[\max_t \text{cond}(\mathbf{J}(t))]). \tag{28}$$

3.4.5 Material Stress from Internal Forces

To ensure a valid solution from the point of robot dynamics, internal forces in the leg chains are calculated according to Sec. 2.4. The force and moment in link j of leg chain i are combined in the wrench vector $\mathbf{w}_{i,j}^{\text{T}} = [\mathbf{f}_{i,j}^{\text{T}}, \mathbf{m}_{i,j}^{\text{T}}]$, as depicted in Fig. 3. The location of the maximum mechanical stress of each link is assumed to be proximal to the base and is calculated, simplified by neglecting torsional and shear

stress, with

$$\sigma_{i,j} = \max_t \|\mathbf{f}_{i,j}\|/A_0 + \|\mathbf{m}_{i,j}\|/W, \tag{29}$$

where $A_0 = \text{const}$ is the sectional area and $W = \text{const}$ is the resistance moment, which are depending on the link geometry and are not subject to optimization. The number

$$k_{\text{stress}} = \max_{i,j} \frac{\sigma_{i,j}}{\sigma_{\max}} \tag{30}$$

describes the maximum relative exceedance of the yield stress $\sigma_{\max}$ of the material for all links of the parallel robot and results in the penalty value

$$v_{\text{stress}} = f_{\text{Norm}}(k_{\text{stress}} - 1) \quad \text{for} \quad k_{\text{stress}} > 1. \tag{31}$$

4 Simulation Results

In the following, first simulative results for the optimization scheme from Sec. 3 are presented. The dimensional synthesis of two architectures of parallel robots with full mobility in two variants each is performed. A detailed description of the simulation scenario and the robot parametrization is presented in Sec. 4.1. The functionality of the hierarchical constraints and the convergence of the optimization is verified in Sec. 4.2. An analysis on the use of the material stress constraint is performed in Sec. 4.3 and the influence of tilting angles on the overall outcome of the optimization is investigated in Sec. 4.4.

4.1 Scenario

The architectures for the dimensional synthesis are the 6PRRS and 6RRRS PKM, shown in Fig. 5,a,c, where "6" marks the number of leg chains, "R" denotes a revolute, "P" a prismatic, "S" a spherical joint and the underscore marks the actuation. The generality of the kinematics and dynamics model laid out in Sec. 2 is highlighted by comparing two different variants of each architecture: One robot with leg chains ending in spherical joints (S), Fig. 5,a,c, and one with leg chains ending in three distinctive revolute joints (RRR), Fig. 5,b,d.

The optimization was performed with the MATLAB-implementation of the particle swarm optimization [23] with 30 generations and 100 particles using the methods described in Sec. 2 and Sec. 3.

All robot links were assumed to be thin tubes (hollow cylinders) with diameter 13 mm and material thickness of 0.8 mm. The moving platform is assumed to be a circular disk with a thickness of 10 mm and the parts to be of aluminum alloy AlCu4PbMgMn.

The leg chains are the result of a structural synthesis [10] and are part of a minimal set of serial-link kinematic chains. This results in a very general description of the kinematics with many free DH-parameters (in the modified notation of Khalil [17]), with only the DH-parameters

$$\alpha_{1,\text{DH}} = 0, \quad \alpha_{5/6,\text{DH}} = \pi/2, \quad d_{6,\text{DH}} = 0 \tag{32}$$

set constant for all robots. For the architecture I (6PRRS), the DH-Parameters $a_5/a_6/d_5$ of the last two joints are set to zeros to model the S-joint. All other parameters are subject to optimization, resulting in 15 variable kinematic parameters

$$\begin{aligned}\mathbf{p}_{\text{kin,I}} = [&d_{\text{base}}, d_{\text{plf}}, \theta_{1,\text{DH}}, \alpha_{2,\text{DH}}, a_{2,\text{DH}}, d_{2,\text{DH}}, \alpha_{3,\text{DH}},\\ &a_{3,\text{DH}}, d_{3,\text{DH}}, \alpha_{4,\text{DH}}, a_{4,\text{DH}}, d_{4,\text{DH}},\\ &d_{\text{basepairdist}}, d_{\text{plfpairdist}}, \alpha_{\text{Pyr}}]^{\text{T}}\end{aligned} \tag{33}$$

and 16 optimization parameters (including the scaling parameter p_{scale}), as elaborated in Sec. 3.2. The variant II (6PRRRRR) without spherical joints has three additional kinematic parameters, yielding

$$\mathbf{p}_{\text{kin,II}} = [\mathbf{p}_{\text{kin,I}}^{\text{T}}, a_{5,\text{DH}}, d_{5,\text{DH}}, a_{6,\text{DH}}]^{\text{T}} \tag{34}$$

and 19 optimization parameters. For architecture III (6RRRS), a simplified base and platform coupling of the leg chains is selected, leaving only 12 optimization parameters, including the scaling parameter, and

$$\begin{aligned}\mathbf{p}_{\text{kin,III}} = [&d_{\text{base}}, d_{\text{plf}}, \alpha_{2,\text{DH}}, a_{2,\text{DH}}, d_{2,\text{DH}}, \alpha_{3,\text{DH}},\\ &a_{3,\text{DH}}, d_{3,\text{DH}}, \alpha_{4,\text{DH}}, a_{4,\text{DH}}, d_{4,\text{DH}}]^{\text{T}}.\end{aligned} \tag{35}$$

Dissolving the S joint into revolute joints gives variant IV (6RRRRRR) and again adds three parameters:

$$\mathbf{p}_{\text{kin,IV}} = [\mathbf{p}_{\text{kin,III}}^{\text{T}}, a_{5,\text{DH}}, d_{5,\text{DH}}, a_{6,\text{DH}}]^{\text{T}}. \tag{36}$$

The parallel robots have to execute a reference cube trajectory in the center of the workspace with an edge length of 30 mm, visible in Fig. 5. The tilting angles of the end effector are increased from 0° to a maximum value depending on the evaluation. To make demands on the robot dynamics, which is the basis for the optimization criterion (energy), the corners of the cube are connected with rest-to-rest motions with a trapezoid profile in acceleration.

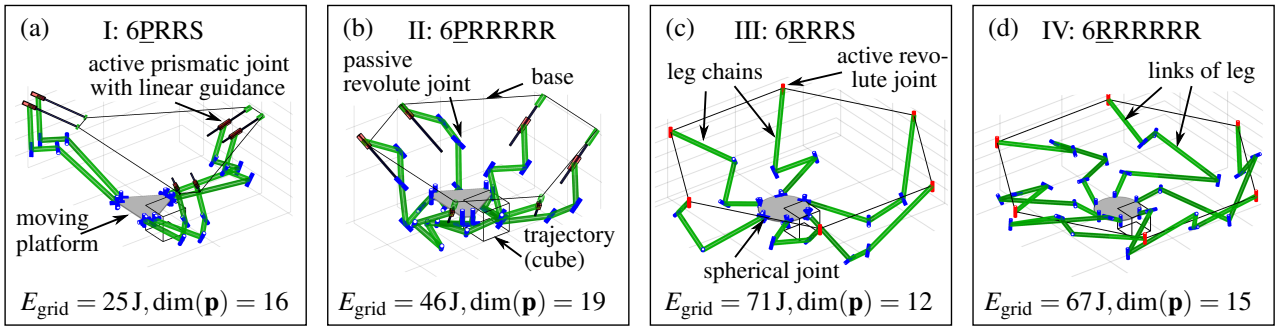

Figure 5 Results of the dimensional synthesis of four robots with objective function E_{grid} and number of parameters $\dim(\mathbf{p})$.

4.2 Convergence and Distribution

The distribution of the values of the fitness function of Fig. 4 for a typical run of the optimization is shown as a histogram in Fig. 6 at the example of the 6RRRS. The fitness values correspond to the constraint violation terms in Fig. 6, described in Sec. 3.4. Blue parts of the bars represent particles from the last generation of the PSO and green parts represent the first generations. By the qualitative distribution of "good" particles (on the left) at the end of the optimization (blue) and "bad" particles (at the right) at the beginning (green), a convergence of the optimization to "good" solutions can be concluded.

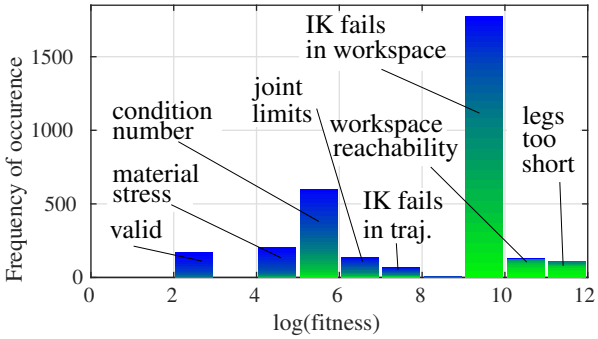

Figure 6 Histogram of the fitness function values f of all particles for one optimization of 6RRRS with generation highlight.

A box-plot of the computation time necessary to calculate the fitness function in Fig. 7 proves that the idea of hierarchical constraints works in principle: Particles violating severe constraints are excluded earlier and need less computation time than better solutions. The box-plots are ordered in classes corresponding to the bars in Fig 6. The spread in computation times can be explained by the gradient-based inverse kinematics.

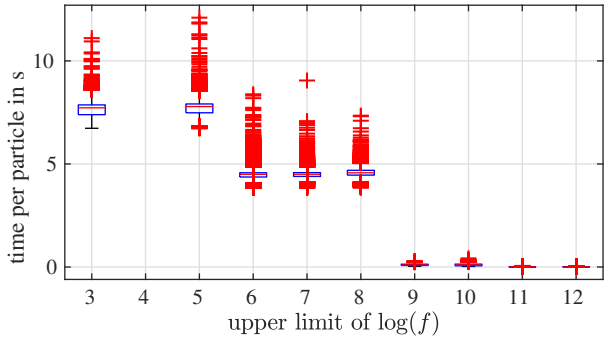

Figure 7 Box-plot of computation times of the particles of P6RRRS in multiple repetitions corresponding to bars in Fig 6.

4.3 Condition and Material Stress

Fig. 8 shows that for the relatively lightweight link geometries the technical limit of the material stress in the final results of multiple runs is nearly reached. It is known that ill-conditioned Jacobian matrices may produce high joint velocities or forces [3]. From this it can be assumed that high condition numbers correlate with high material stress and the test of the condition number from Sec. 3.4.4 as a constraint would be sufficient. The distribution of the material stress in Fig. 8 shows that a strong correlation of Jacobian condition number and material stress is not evident. Therefore it can be concluded that under the mentioned conditions the consideration of the material stress constraint is useful, yet unusual in literature on dimensional synthesis.

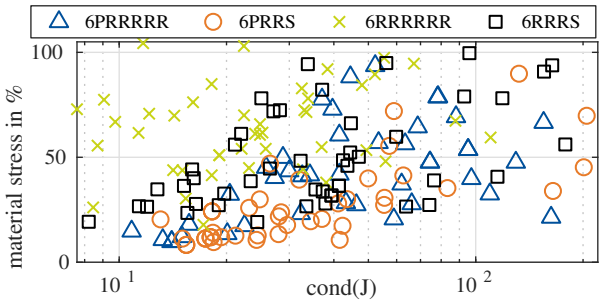

Figure 8 Relation of material stress and Jacobian condition number (in logarithmic scale) for low tilting angles of about 10°.

4.4 Evaluation of Tilting Angles

The distribution of final results of multiple runs of the optimization is shown in Fig. 9 and Fig. 10 for different maximal tilting angles in the reference trajectory. The robots with an S joint seem to perform better than the ones without, as can be summarized from their lower Energy consumption (i.e. objective of the optimization) in Fig. 9. The higher number of markers for the S joint PKM represents their higher ratio of successful runs of the optimization.

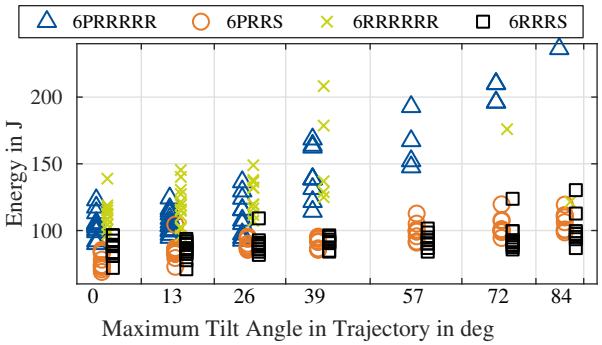

Figure 9 Comparison of optimization results in different maximum tilt angles of the cube trajectory. Horizontal axes values are shifted from -1.5 to 1.5 for facility of inspection and the results are grouped according to the tilting angle.

On the contrary, the structures with three R joints instead of one S joint seem to have a tendency for lower condition number in the final results, as can be seen in Fig. 10.

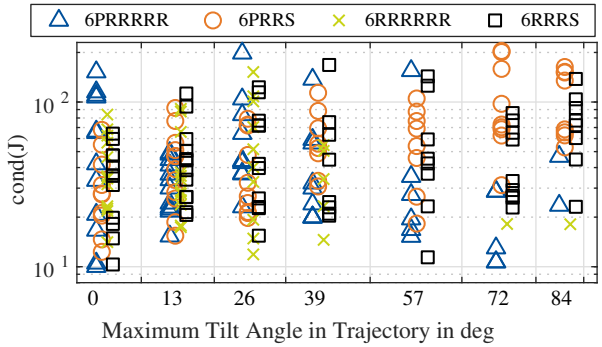

Figure 10 Worst condition numbers for the results from Fig. 9.

5 Summary and Outlook

A general methodology for the modeling and dimensional synthesis of parallel robots is presented, which differs from similar work by being applicable to non-classical parallel robots, the use of a single-objective optimization, the concepts of hierarchical constraints and consumed energy as objective. Further work will extend the constraint formulation by considering self-collisions and additional plausibility checks. Future research will cover comparing robots with and without task redundancy as well as integrating the design optimization of link geometry and drive selection.

6 Acknowledgement

The authors acknowledge the support by the Deutsche Forschungsgemeinschaft (DFG) under grant OR 196/33-1. MATLAB Code to reproduce the results is available at GitHub under https://github.com/SchapplM/robsynth-paper_iftommdach2020.

7 References

[1] Kong, X., Gosselin, C.M.: *Type synthesis of parallel mechanisms*. Springer Berlin Heidelberg (2007). DOI 10.1007/978-3-540-71990-8

[2] Gogu, G.: *Structural synthesis of parallel robots, part 1: methodology*, *Solid Mechanics and Its Applications*, vol. 866. Springer Netherlands (2008). DOI 10.1007/978-1-4020-5710-6

[3] Merlet, J.P.: *Parallel robots*, *Solid Mechanics and Its Applications*, vol. 128, 2nd edn. Springer Science & Business Media (2006). DOI 10.1007/1-4020-4133-0

[4] Krefft, M.: *Aufgabenangepasste Optimierung von Parallelstrukturen für Maschinen in der Produktionstechnik*. Ph.D. thesis, Technische Universität Braunschweig (2006)

[5] Carbone, G., Ottaviano, E., Ceccarelli, M.: *An optimum design procedure for both serial and parallel manipulators*. Proceedings of the Institution of Mechanical Engineers Part C Journal of Mechanical Engineering Science **221**(7), 529–843 (2007). DOI 10.1243/0954406JMES367

[6] Frindt, M.: *Modulbasierte Synthese von Parallelstrukturen für Maschinen in der Produktionstechnik*. Ph.D. thesis, TU Braunschweig (2001)

[7] Mbarek, T., Nefzi, M., Corves, B.: *Prototypische Entwicklung und Konstruktion eines neuartigen Parallelmanipulators mit dem Freiheitsgrad fünf*. VDI-Berichte (2005)

[8] Frindt, M., Krefft, M., Hesselbach, J.: *Structure and type synthesis of parallel manipulators*. In: Robotic Systems for Handling and Assembly, p. 17ff. Springer (2010). DOI 10.1007/978-3-642-16785-0_2

[9] Schappler, M., Tappe, S., Ortmaier, T.: *Modeling parallel robot kinematics for 3T2R and 3T3R tasks using reciprocal sets of Euler angles*. MDPI Robotics **8**(3) (2019). DOI 10.3390/robotics8030068

[10] Ramirez, D.A.: *Automatic generation of task-specific serial mechanisms using combined structural and dimensional synthesis*. Ph.D. thesis, Gottfried Wilhelm Leibniz Universität Hannover (2018). DOI 10.15488/4571

[11] Stock, M., Miller, K.: *Optimal kinematic design of spatial parallel manipulators: application to linear delta robot*. J. Mech. Des. **125**(2), 292–301 (2003). DOI 10.1115/1.1563632

[12] Kelaiaia, R., Company, O., Zaatri, A.: *Multiobjective optimization of a linear Delta parallel robot*. Mechanism and Machine Theory **50**(0), 159–178 (2012). DOI 10.1016/j.mechmachtheory.2011.11.004

[13] Jamwal, P.K., Hussain, S., Xie, S.Q.: *Three-stage design analysis and multicriteria optimization of a parallel ankle rehabilitation robot using genetic algorithm*. IEEE Transactions on Automation Science and Engineering **12**(4), 1433–1446 (2015). DOI 10.1109/TASE.2014.2331241

[14] Zhou, L., Bai, S., Hansen, M.R.: *Design optimization on the drive train of a light-weight robotic arm*. Mechatronics **21**(3), 560–569 (2011). DOI 10.1016/j.mechatronics.2011.02.004

[15] Zhou, L., Bai, S.: *A new approach to design of a lightweight anthropomorphic arm for service applications*. Journal of Mechanisms and Robotics **7**(3), 031,001 (2015). DOI 10.1115/1.4028292

[16] Briot, S., Khalil, W.: *Dynamics of parallel robots*, *Mechan. Machine Science*, vol. 35. Springer (2015). DOI 10.1007/978-3-319-19788-3

[17] Khalil, W., Dombre, E.: *Modeling, identification and control of robots*. Hermes Penton Science (2002). DOI 10.1016/B978-1-903996-66-9.X5000-3

[18] Abdellatif, H., Heimann, B.: *Computational efficient inverse dynamics of 6-DOF fully parallel manipulators by using the Lagrangian formalism*. Mechanism and Machine Theory **44**(1), 192–207 (2009). DOI 10.1016/j.mechmachtheory.2008.02.003

[19] Do Thanh, T., Kotlarski, J., Heimann, B., Ortmaier, T.: *On the inverse dynamics problem of general parallel robots*. In: IEEE International Conference on Mechatronics 2009, pp. 1–6 (2009). DOI 10.1109/ICMECH.2009.4957202

[20] Samin, J.C., Fisette, P.: *Symbolic modeling of multibody systems*, *Solid Mechanics and Its Applications*, vol. 112. Springer Science & Business Media (2013). DOI 10.1007/978-94-017-0287-4

[21] Khalil, W., Guegan, S.: *Inverse and direct dynamic modeling of Gough-Stewart robots*. IEEE Transactions on Robotics **20**(4), 754–761 (2004). DOI 10.1109/TRO.2004.829473

[22] Jordehi, A.R.: *A review on constraint handling strategies in particle swarm optimisation*. Neural Computing and Applications **26**(6), 1265–1275 (2015). DOI 10.1007/s00521-014-1808-5

[23] The MathWorks, Inc.: *Particle swarm*. URL https://de.mathworks.com/help/gads/particleswarm.html. Accessed 11.02.2020

DOI: 10.17185/duepublico/71211
URN: urn:nbn:de:hbz:464-20200221-114151-1